A Decentralized Control Architecture Applied to DC Nanogrid Clusters for Rural Electrification in Developing Regions

Mashood Nasir, Zheming Jin, *Student Member, IEEE*, Hassan A. Khan, *Member, IEEE*, Nauman Ahmad Zaffar, *Member, IEEE*, Juan C. Vasquez, *Senior Member, IEEE*, and Josep M. Guerrero, *Fellow, IEEE*

***Abstract*—DC microgrids built through a bottom-up approach are becoming popular for swarm electrification due to their scalability and resource-sharing capabilities. However, they typically require sophisticated control techniques involving communication among the distributed resources for stable and coordinated operation. In this work, we present a communication-less strategy for the decentralized control of a photovoltaic (PV)/battery-based highly distributed dc microgrid. The architecture consists of clusters of nanogrids (households), where each nanogrid can work independently along with provisions of sharing resources with the community. An adaptive *I–V* droop method is used, which relies on local measurements of state of charge and dc bus voltage for the coordinated power sharing among the contributing nanogrids. PV generation capability of individual nanogrids is synchronized with the grid stability conditions through a local controller, which may shift its modes of operation between maximum power point tracking mode and current control mode. The distributed architecture with the proposed decentralized control scheme enables 1) scalability and modularity in the structure, 2) higher distribution efficiency, and 3) communication-less, yet coordinated resource sharing. The efficacy of the proposed control scheme is validated for various possible power-sharing scenarios using simulations on MATLAB/Simulink and hardware-in-the-loop facilities at the Microgrid Laboratory, Aalborg University.**

***Index Terms*—DC microgrid, dc nanogrid, distributed generation, distributed storage, droop control, rural-electrification.**

I. Introduction

ACCORDING to the International Energy Agency, around 1.2 billion people (16% of the global population) do not

Manuscript received December 5, 2017; revised February 28, 2018; accepted April 6, 2018. Date of publication April 18, 2018; date of current version December 7, 2018. This work was supported by the International Research Support Initiative Program by Higher Education Commission of Pakistan and collaborated between the Department of Electrical Engineering, Lahore University of Management Sciences, and the Department of Energy Technology, Aalborg University. Recommended for publication by Associate Editor K. Sun. *(Corresponding author: Mashood Nasir.)*

M. Nasir, H. A. Khan, and N. A. Zaffar are with the Department of Electrical Engineering, Lahore University of Management Sciences, Lahore 54792, Pakistan (e-mail:

modular nature. Furthermore, distribution efficiency is a major limitation for centralized architectures, as distribution losses become significant at low distribution voltages, thin conductor sizes, and higher power levels [13]. Moreover, such architectures require relatively higher initial capital investment due to top-down sizing requirements [14].

Various distributed architectures for PV/battery-based islanded dc microgrids have been proposed in the literature. Distributed architectures with the bottom-up approach enable organic growth of a microgrid, thereby empowering local communities for sustainable development [14]. Inam *et al.* [15] presented a partially distributed architecture, in which peer-to-peer electricity sharing was enabled by GSM based on power management units. Similarly, Madduri *et al.* [16], [17] proposed a PV/battery-based central generation and distributed storage architecture, with the provision of local batteries in individual households. The advantages of distributed architectures are mainly reduction in distribution losses and modularity in the structure. However, coordinated power sharing among the distributed resources becomes extremely challenging. Several strategies for hierarchical and supervisory control of dc microgrids have been proposed in [18]–[21]. However, these require an extra layer of sensing and communication, which enhances the cost and complexity of the system.

Thus, for PV/battery-based rural electrification, a distributed architecture having minimum distribution losses, modularly scalable structure, and communication-less control is highly desirable. Nasir *et al.* [22] presented a PV-based distributed generation and distributed storage architecture (DGDSA) of a dc microgrid for rural electrification. However, the hysteretic-based voltage droop algorithm presented in [22] depends upon the perturbations in duty cycle. A very small perturbation in duty makes the dynamics of a system very slow to achieve the desired power sharing, while a higher perturbation in duty cycle may lead to instability. In such a scheme, resource-sharing capability among the distributed resources is uncoordinated, i.e., all nanogrids share or demand uniform amount of power regardless of their current states generation and storage.

Lu *et al.* [23] developed an adaptive dual-loop droop control (inner current loop and outer voltage loop) on the basis of state of charge (SOC) balancing. This adaptive droop considers power sharing proportional to the battery SOC index during a power supply mode (battery discharge mode). However, it does not consider power sharing in proportion to the SOC index during the charging mode of the battery. Therefore, all batteries get charged with the same power independent of their SOC or resource availability for battery charging. If such a scheme is applied on the DGDSA of the dc microgrid presented in [22] having local loads, there will be redundant distribution losses for unwanted SOC balancing. Ideally, in such architectures, it is desirable that if SOC is above a certain threshold, it must be maintained to that level rather than undesired balancing. Moreover, Jin *et al.* [24] showed that the *V–I* dual-loop droop control exhibits slower dynamics in comparison to *I–V* droop; therefore, it cannot achieve fast power sharing among the distributed resources.

Therefore, in order to rectify these limitations of decentralized control schemes for distributed dc microgrids, we present an adaptive *I–V* droop method for the decentralized control of a PV-based DGDSA of the dc microgrid suitable for rural electrification. The resource sharing among the contributing nanogrids is kept in proportion to the availability of resources for both operation modes, i.e., during supply and demand of the power to or from the nanogrid (charging and discharging of the battery). This power sharing proportional to resource availability is achieved by using an adaptive *I–V* droop algorithm, which may adjust its droop based on the local measurement of dc bus voltage and SOC of the battery. Moreover, the proposed control scheme ensures fast dynamics and is capable to deal with the extreme operating conditions by synchronizing PV generation capability of individual nanogrids with the local load requirements and grid stability conditions through a local controller, which may shift its modes of operation between maximum power point tracking (MPPT) mode and current control mode. Since the proposed control scheme relies on the local measurements of load current, PV generation, battery SOC, and dc bus voltage, therefore does not require communication for the coordinated power sharing among the contributing nanogrids. Thus, with the proposed adaptive control scheme, a PV-based DGDSA combines the advantages of both the existing architectures, i.e., scalability, modularity, lower distribution losses, along with robust, coordinated, and communication-less decentralized control. Thus, such a decentralized system can be considered as an ideal candidate for future deployments of rural electrification projects in developing regions.

The rest of this paper is organized as follows. In Section II, the architecture of the proposed microgrid as an interconnection of multiple nanogrids is presented. In Section III, power electronic interface and control schemes are presented. Section IV presents the objectives for various possible scenarios of coordinated control. Simulation and hardware results are presented in Section V. Based on the results and discussions, a conclusion is drawn in Section VI.

II. Distributed Generation and Distributed Storage Architecture of the DC Microgrid

The combination of PV generation, battery storage, local dc loads, and dc–dc converters in an individual household formulates a nanogrid. Local generation and local storage allow the nanogrid to work independently even if the grid is unavailable and has many practical advantages compared to central generation based systems. A cluster of N multiple nanogrids is interconnected via a dc link to formulate the DGDSA of a dc microgrid, as shown in Fig. 1. An individual nanogrid is, therefore, considered a basic building block, whose modular replication and subsequent dc-link integration yields scalability in the architecture. Each nanogrid operates independently when it is self-sufficient in its resources and resource sharing among multiple nanogrids is enabled only when an individual nanogrid has either access or deficiency of resources. Therefore, energy losses with the distribution of energy in the DGDSA are limited in comparison to other partially distributed or centralized architectures, where generated energy has to be distributed all the way from centralized generation point to individual households [13], [22]. Furthermore, the DGDSA has the capability to aggregate power from multiple nanogrids for driving community loads. The supply of power for large communal loads is other-

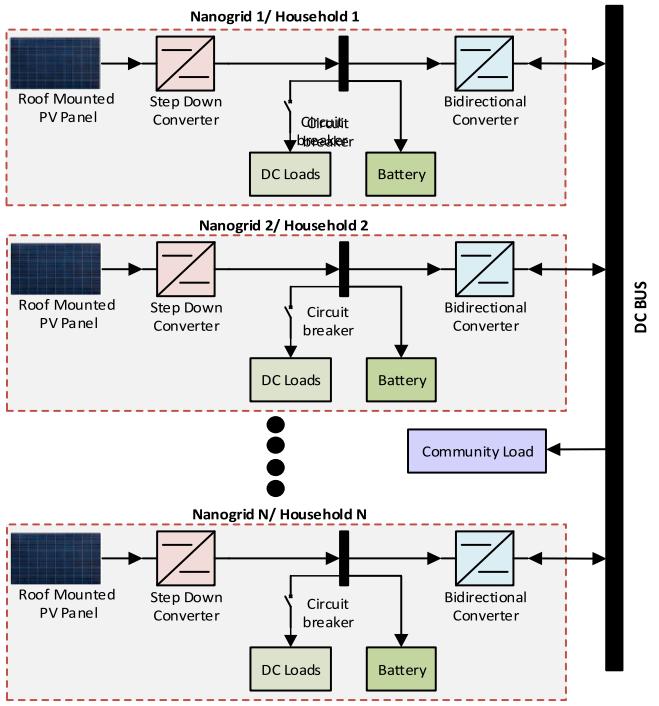

Fig. 1. Cluster of multiple nanogrids interconnected via dc bus formulating the DGDSA of a PV/battery-based dc microgrid.

wise expensive and unsustainable in limited rural electrification projects [13], [22].

III. Proposed Decentralized Control Scheme for Communication-Less and Coordinated Resource Sharing Among the Cluster of Multiple Nanogrids

In the proposed decentralized scheme, each individual nanogrid is responsible for coordinated power sharing among the clusters without any physical communication. Power electronic interface for the formulation of an individual nanogrid is shown in Fig. 2(a), which shows local PV generation, battery storage, household load, and two dc–dc converters for power processing in an individual nanogrid. Index i represents an arbitrary nanogrid in a cluster of N nanogrids. The battery acts as a buffer between converter 1 of the ith nanogrid (Conv1_i) and converter 2 of the ith nanogrid (Conv2_i), and is responsible to keep the voltage fixed at the local bus to which household load is connected. Therefore, the battery acts as a point of common coupling at which the terminals of load and both converters are connected. Conv1_i is an isolated bidirectional converter and is responsible for controlled power sharing among nanogrids through an interconnected dc bus. Distribution voltage in such low-voltage direct current (LVDC) microgrids is dictated by dc bus voltage and is a key factor for achieving optimal distribution efficiency. Distribution at higher voltage is generally more efficient from the perspective of line losses and voltage drops at the rear end [22]. Therefore, dc bus voltage is kept higher in comparison to battery voltage or household load voltage. This is achieved through converter (Conv1_i), which interfaces the battery with the dc bus. Moreover, to enable two-way power flow between the battery of individual nanogrid and dc bus, this converter is made bidirectional in nature, as shown in Figs. 1 and 2. The advantage of making it as an isolated converter is twofold, i.e., 1) it provides isolation between grid and battery and 2) higher ratio of dc–dc voltage conversion can be achieved for implementing higher levels of LVDC, i.e., 120, 230, or 380 V [22]. Converter 2 (Conv2_i) on the other hand is a step-down converter and is responsible for optimal power extraction from PV panels.

The communication-less coordination among the distributed resources is achieved through the simultaneous control of each individual nanogrid via control scheme shown in Fig. 2(b). The control scheme shown in Fig. 2(b) utilizes an adaptive algorithm [shown in Fig. 2(c)], for switching of Conv1_i based on the local measurements of bus voltage V_B and battery state of charge SOC_i. This control scheme is also responsible for switching of Conv2_i among MPPT and current control mode based on the local measurements of household load, PV generation, and battery SOC_i. Various possible modes of operation for Conv1_i and Conv2_i for each individual nanogrid, as shown in Fig. 2(c), are discussed in the following sections.

A. Multimode Adaptive Control Scheme for a Bidirectional Converter ($Conv1_i$) Integrated With a DC Bus

For each nanogrid i, the control mode for its bus-interfaced converter Conv1_i is determined by an adaptive controller on the basis of bus voltage V_B and SOC of its battery SOC_i. SOC_i of the battery is approximated by a simple Coulomb counting method, as governed by (1), and is based on the ideal energy balance at the ith local bus given by (2):

$$\text{SOC}_i(t) = \text{SOC}_i(0) + \frac{1}{C_i}\int_0^T V_i^b\left(I_i^{\text{in}} - I_i^{\text{load}} - I_i^L\right)\,dt \tag{1}$$

$$P_i^{\text{PV}}(t)\,\Delta t = P_i^{\text{load}}(t)\,\Delta t + P_i{}^L(t)\,\Delta t + \int_0^T V_i^b\left(I_i^{\text{in}} - I_i^{\text{load}} - I_i^L\right)\,dt \tag{2}$$

where $\text{SOC}_i(0)$ is the initial SOC for the battery at the ith nanogrid, C_i is its rated energy capacity (Wh), I_i^{in} is the current provided by PV panels after a buck converter (Conv2_i), I_l^{load} is the current demanded by household dc loads, I_i^L is the current supplied by the nanogrid to the dc bus, $P_i^{\text{PV}}(t)$ is the power generated by the PV panel at time t whose rated capacity is $P^{\text{PV}}(W_p)$, $P_i^{\text{load}}(t)$ is the power demanded by household at time t whose rated load capacity is $P^{\text{load}}(W)$, and $V_i^b(t)$ is the time-varying voltage of the battery whose rated voltage is V_b. By convention, I_i^L and P_i^L values are positive when current and power are being supplied by the nanogrid to the dc bus and negative when current and power are being demanded by the nanogrid for household load or battery charging. In order to ensure the coordinated operation along with enhanced battery life time in each individual nanogrid, upper and lower thresholds on the battery SOC (SOC_i) are defined as $\text{SOC}_{\max}$ and $\text{SOC}_{\min}$. SOC_i of the battery is considered as the resource availability index in the ith nanogrid, where a value of SOC_i below $\text{SOC}_{\min}$ indicates that the nanogrid is deficient in resources, a value of SOC_i above or equal to $\text{SOC}_{\max}$ indicates that the nanogrid is saturated in resources, and a value of SOC_i

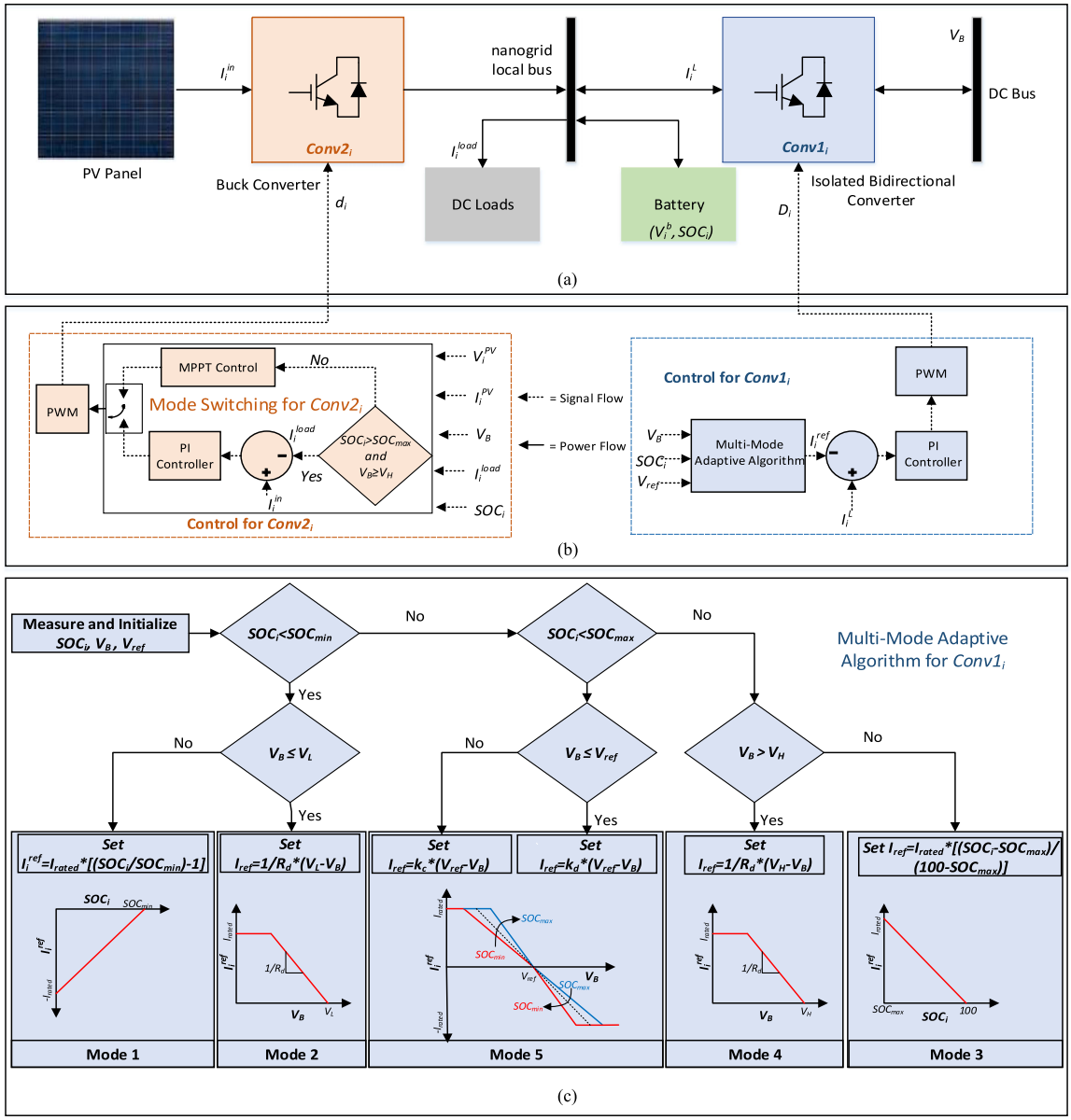

Fig. 2. Power electronic interface and control schemes for an individual nanogrid to achieve the desired decentralized coordinated power sharing. (a) Power stage of the ith nanogrid. (b) Control stage of the ith nanogrid. (c) Multimode adaptive algorithm used in the control stage of Conv1 at the ith nanogrid.

in between $\mathrm{SOC}_{\max}$ and $\mathrm{SOC}_{\min}$ indicates that the nanogrid is self-sufficient. Similarly, in order to ensure the stability of the microgrid, a hysteresis is kept in the bus voltage V_B such that it is allowed to vary in between $\pm 5\%$ of the rated bus voltage V_{ref}, and associated higher and lower limits of voltage are denoted as V_H and V_L, respectively. The local measurement of V_B at individual nanogrid serves as an indication for resource availability in the overall microgrid structure, where a value lower than V_L indicates that the cluster is deficient in resources, a value higher than or equal to V_H indicates that the cluster is already saturated, and a value in between V_L and V_H indicates that the cluster has the capability of supplying as well as demanding power. Based on the local measurements of SOC and V_B, an adaptive algorithm is used for the calculation of I_i^{ref} given by (4)–(11) and shown in Fig. 2(c). An inner loop current control is then used to control the current of $\mathrm{Conv1}_i$ (I_i^L) through a PI controller that generates the duty cycle D_i given by (3), where k_p and k_i are the proportional and integral constants for the PI controller, respectively. Based on the local measurements of SOC_i and V_B, $\mathrm{Conv1}_i$ of the ith nanogrid can switch in the following modes as highlighted in Fig. 2(c):

$$D_i = k_p \left(I_i^{\mathrm{ref}} - I_i^L\right) + k_i \int_0^t \left(I_i^{\mathrm{ref}} - I_i^L\right) dt. \tag{3}$$

1) Mode 1: Nanogrid Is Deficient in Resources, While the Cluster Has Sufficient Resource Availability: A value of SOC_i below $\mathrm{SOC}_{\min}$ indicates that the ith nanogrid is deficient in resources and any further discharge below this point will deteriorate the battery life. So, individual household loads are shut down with a relay and it starts absorbing power to achieve the minimum sustainability level, i.e., $\mathrm{SOC}_{\min}$. A value of V_B higher than reference voltage V_{ref} indicates that neigh-

boring nanogrids have enough capability to serve for the demand of resource-deficient nanogrids. In this situation, resource-deficient nanogrids will demand power in accordance to their resource deficiency. The current reference I_i^{ref} varies with SOC_i in a linear fashion from $\text{SOC}_i = 0$ to $\text{SOC}_{\min}$, as shown in Fig. 2(c) (mode 1), and is given by (4). From (4) and Fig. 2(c) (mode 1), it is evident that the battery of the resource-deficient nanogrid will get charged with rated current I_{rated} at $\text{SOC}_i = 0$, and power delivery will become eventually zero with $I_i^{\text{ref}} = 0$ as SOC_i approaches to $\text{SOC}_{\min}$, where I_{rated} is the rated charging current for the battery, specified by manufacturer datasheet

$$I_i^{\text{ref}} = I_{\text{rated}} \left(\frac{\text{SOC}_i}{\text{SOC}_{\min}} - 1 \right) \quad \forall i \in [1, N] \text{ if } V_B > V_L. \tag{4}$$

2) Mode 2: Nanogrid and Cluster, Both Are Deficient in Resources: A value of SOC_i below $\text{SOC}_{\min}$ and $V_B \leq V_L$ indicates that the ith nanogrid is deficient in resources, while neighboring nanogrids in the cluster do not have the capability to serve for the demand of resource-deficient nanogrids. Therefore, to avoid any further drop in dc bus voltage, each Conv1_i will adjust its reference current to stabilize dc bus voltage at lower allowable limit, i.e., V_L. This coordination is achieved through the virtual droop resistance R_d of the converter and is given by (5) [also shown in Fig. 2(c) (mode 2)]. From (5) and Fig. 2(c) (mode 2), it is evident that once dc bus voltage stabilizes at lower allowable limit, i.e., V_L, net exchange of the power between multiple nanogrids will become zero with $I_i^{\text{ref}} = 0$

$$I_i^{\text{ref}} = \frac{1}{R_d} (V_L - V_B) \quad \forall i \in [1, N] \text{ if } V_B \leq V_L. \tag{5}$$

3) Mode 3: Nanogrid Is Saturated, While the Cluster Is Unsaturated in Resources: A value of SOC_i higher than $\text{SOC}_{\max}$ indicates that the ith nanogrid has very high resource availability and it needs to supply power to the neighboring nanogrids. If the bus voltage V_B is lower than V_H, it indicates that the cluster is unsaturated in resources, and neighboring nanogrids can absorb power; therefore, each Conv1_i will supply power to the cluster. The current reference I_i^{ref} varies with SOC_i in a linear fashion from $\text{SOC}_{\max}$ to $\text{SOC} = 100\%$, as shown in Fig. 2(c) (mode 3) and is given by (6). From (6) and Fig. 2(c) (mode 3), it is evident that the battery of the saturated nanogrid will be discharged with rated current I_{rated} at $\text{SOC}_i = 100$, and the power delivery will become eventually zero with $I_i^{\text{ref}} = 0$ as SOC_i approaches to $\text{SOC}_{\max}$

$$I_i^{\text{ref}} = I_{\text{rated}} \left(\frac{\text{SOC}_i - \text{SOC}_{\max}}{100 - \text{SOC}_{\max}} \right) \quad \forall i \in [1, N] \text{ if } V_B < V_H. \tag{6}$$

4) Mode 4: Nanogrid and Cluster, Both are Saturated in Resources: A value of SOC_i above $\text{SOC}_{\max}$ and V_B higher than or equal to V_H indicates that the ith nanogrid is saturated in resources, while neighboring nanogrids in the cluster are already saturated. Therefore, under this condition, to avoid increase in dc bus voltage, each Conv1_i will adjust its reference current to stabilize dc bus voltage at higher allowable limit, i.e., V_H. This coordination is achieved through the virtual droop resistance R_d of the converter and is given by (7) [also shown in Fig. 2(c) (mode 4)]. From (7) and Fig. 2(c) (mode 2), it is evident that once dc bus voltage stabilizes at higher allowable limit, i.e., V_H, and net exchange of power between multiple nanogrids will become zero with $I_i^{\text{ref}} = 0$

$$I_i^{\text{ref}} = \frac{1}{R_d} (V_H - V_B) \quad \forall i \in [1, N] \text{ if } V_B \geq V_H. \tag{7}$$

5) Mode 5: Nanogrid Is Self-Sufficient, While the Cluster Can Supply or Demand Resources: For the ith nanogrid, the value of SOC_i in between $\text{SOC}_{\max}$ and $\text{SOC}_{\min}$ indicates that it is self-sufficient in resources. Under this condition, it can either supply power to the cluster, it can demand power from the cluster, or it can work independently without any exchange of power among the neighboring nanogrids in the cluster. If all the nanogrids in the cluster are self-sufficient, there is no exchange of power among neighboring nanogrids and voltage is stabilized at V_{ref} through adaptive *I–V* droop control.

A value of V_B higher than V_{ref} indicates that number of power supplying nanogrids in the cluster is more than number of power demanding nanogrids; therefore, the ith nanogrid needs to absorb power to keep the microgrid stable. The coordinated power absorption under this condition is achieved through an adaptive *I–V* droop control given by (8) and shown in Fig. 2(c) (mode 5). Rather than having a fixed value of droop resistance, a charging droop coefficient K_c has been defined as a function of droop resistance R_d and SOC_i given by (9). For $\text{SOC}_{\min} < \text{SOC}_i < \text{SOC}_{\max}$

$$I_i^{\text{ref}} = K_c (V_{\text{ref}} - V_B) \quad \forall i \in [1, N] \text{ if } V_B > V_{\text{ref}} \tag{8}$$

$$K_c (R_d, \text{SOC}_i) = \frac{1}{R_d} \left(2 - \frac{\text{SOC}_i - \text{SOC}_{\min}}{\text{SOC}_{\max} - \text{SOC}_{\min}} \right). \tag{9}$$

A higher value of droop coefficient at $\text{SOC}_{\min}$ and a lower value of droop coefficient at $\text{SOC}_{\max}$ result in a coordinated power absorption such that the nanogrid with the lowest SOC absorbs the highest amount of power from the cluster and vice versa. The proposed scheme employs an adaptive *I–V* droop method for the control of the microgrid. Although current-based droop control (*I–V* droop) exhibits better transient performance in comparison to other droop methods (e.g., *V–I* droop); however, it may be subjected to instability, if droop coefficient is kept too high [25]. The upper and lower boundary conditions for the stability of *I–V* droop controlled microgrids and a design criterion for global droop coefficient ensuring system stability for wide range operation have been discussed in [25]. It has been shown that stability margins of the system increase with the increase in dc-link capacitance, decrease in feeder inductance, and decrease in load power [25]. Since the proposed distribution architecture is designed for the limited electrification needs of rural occupants with smaller distribution radius (standard size of a village is less than a km), therefore due to high link capacitance, low feeder inductance, and low power loads, stability margins are relatively higher. The droop coefficient in the proposed adaptive scheme has been varied linearly from $2/R_d$ to $1/R_d$ between $\text{SOC}_{\min}$ and $\text{SOC}_{\max}$ and lies within the stable boundaries, as discussed in [25]. Other linear and nonlinear variations of droop function can be considered in the proposed approach without losing stability, subject to the conditions for droop coefficient design in [25].

A value of V_B lower than V_{ref} indicates that number of power demanding nanogrids in the cluster is more than number of

power supplying nanogrids, or there is a communal load demand; therefore, the ith nanogrid needs to supply power to keep the microgrid stable. The coordinated power sharing among the supplying nanogrids is ensured through modified *I–V* droop control given by (10) and shown in Fig. 2(c) (mode 5). For this range, a discharging droop coefficient K_d has been defined based on the same criteria discussed earlier

$$I_i^{\text{ref}} = K_d\left(V_{\text{ref}} - V_B\right) \quad \forall i \in [1, N] \text{ if } V_B \leq V_{\text{ref}} \tag{10}$$

$$K_d\left(R_d, \text{SOC}_i\right) = \frac{1}{R_d}\left(1 + \frac{\text{SOC}_i - \text{SOC}_{\min}}{\text{SOC}_{\max} - \text{SOC}_{\min}}\right). \tag{11}$$

The variations in droop coefficient with SOC_i ensure that the nanogrid with the highest resource availability (higher value of SOC) will supply more power in comparison to the nanogrid having a relatively lower value of SOC.

B. Scheme for Switching Between MPPT and Current Control Modes for the Converter Integrated With the PV Panel (Conv2$_i$)

The buck converter of each nanogrid (Conv2_i) at the output of the PV panel is responsible for optimal battery charging. MPPT control is widely used in PV-based systems for the extraction of the maximum power output of incident solar energy. Various schemes for MPPT under uniform and nonuniform irradiance have been discussed in the literature [26], [27]. In this paper, the perturb and observe algorithm is employed due to its simplicity and low computational complexity [26]. The algorithm processes PV panel voltage V_i^{PV} and current I_i^{PV} to generate duty cycle *di* for the maximum power extraction from the PV panel at a given solar irradiance. In most of its operation range, Conv2_i will operate in the MPPT mode; however, based on the measurements of SOC_i and V_B, Conv2_i may shift its operation from the MPPT mode to the inner loop current control mode to culminate its power generation from MPPT to household load current requirements I_i^{load} only. Thus, for $\text{SOC}_i > \text{SOC}_{\max}$ and $V_B \geq V_H$, Conv2_i will operate in the inner loop current control mode through a PI controller that will generate duty cycle d_i given by the following equation, where k'_P and k'_i are proportional and integral constants of PI controllers employed for the control of Conv2_i

$$d_i = k'_p\left(I_i^{\text{load}} - I_i^{\text{in}}\right) + k'_i \int_0^t \left(I_i^{\text{load}} - I_i^{\text{in}}\right)\, dt. \tag{12}$$

IV. Objectives for Stable and Coordinated Operation

For stable operation of the microgrid, dc bus voltage V_B must be maintained to rated value V_{ref} with some allowed fluctuation ($\pm 5\%$) in bus voltage for all possible operating conditions. The other control objective is to minimize the overall distribution losses while maintaining a coordinated resource sharing among the nanogrids. The proposed decentralized scheme will ensure the stable and coordinated operation in the following possible scenarios.

1) Each nanogrid is self-sufficient in its resources, i.e., PV generation/battery cushion is in accordance with household load requirements, and any exchange of power among nanogrids is not desirable to minimize the distribution losses. This will be achieved through the operation of each Conv1_i in mode 5 and each Conv2_i in the MPPT mode.
2) Although each nanogrid is self-sufficient in its resources, there is a communal load demand on the microgrid. In this case, it is desirable that each individual nanogrid contribute power for communal load operation in proportion to its resources availability. This will be achieved through the operation of each Conv1_i in mode 5 and each Conv2_i in the MPPT mode.
3) Out of total *N* nanogrids, *K* nanogrids are self-sufficient, while $N - K$ nanogrids are deficient in resources. In this case, it is desirable that *K* self-sufficient nanogrids share their resources with the remaining $N - K$ resource-deficient nanogrids in a coordinated fashion such that the nanogrid with the highest resource availability should supply more power in comparison to the rest of self-sufficient nanogrids and the nanogrid with the highest resource deficiency should receive more power in comparison to the rest of deficient nanogrids. In this situation, Conv1_i of *K* self-sufficient nanogrids will be operating in mode 5, while remaining $N - K$ nanogrids will be operating in mode 1. Conv2_i of all *N* nanogrids will be operating in the MPPT mode.
4) Out of total *N* nanogrids, *K* nanogrids are self-sufficient, while $N - K$ nanogrids are deficient in resources and there is a communal load demand. In this case, it is desirable that *K* self-sufficient nanogrids share their resources with the remaining $N - K$ resource-deficient nanogrids in a coordinated fashion and communal load demand is also met such that the nanogrid having the highest resource availability supply more power and vice versa. In this situation, Conv1_i of *K* self-sufficient nanogrids will be operating in mode 5, while remaining $N - K$ nanogrids will be operating in mode 1. Conv2_i of all *N* nanogrids will be operating in the MPPT mode.
5) Out of total *N* nanogrids, *K* nanogrids are self-sufficient, while $N - K$ nanogrids are saturated in resources. In this case, it is desirable that *K* self-sufficient nanogrids absorb power from the remaining $N - K$ resource saturated nanogrids in a coordinated fashion such that the nanogrid with the lowest resource availability absorb more power and vice versa. In this situation, Conv1_i of *K* self-sufficient nanogrids will be operating in mode 5, while remaining $N - K$ nanogrids will be operating in mode 3. Conv2_i of all *N* nanogrids will be operating in the MPPT mode.
6) All the nanogrids are generating more power than their local requirements, i.e., excess power is available after fulfilling household load requirements and battery capacity. Although this situation can be largely avoided by optimally designing PV generation and battery storage resources [28]. Still, even a single occurrence of this situation may instigate grid instability. In this case, it is desirable to culminate the PV generation and synchronize it with household load requirements. In this situation, Conv1_i of all *N* nanogrids will be operating in mode 4 and Conv2_i of all *N* nanogrids will be operating in a current control mode.
7) All nanogrids are deficient in resources and they start demanding power, which may result in grid voltage drop

TABLE I
PARAMETERS OF SIMULATED CASE STUDY

Description of the Parameter	Symbol	Value	Description of the Parameter	Symbol	Value
No. of Nanogrids/ households	N	4	Maximum threshold of battery *SOC*	SOC_{max}	80%
DC bus capacitance	C_B	10mF	Minimum threshold of battery *SOC*	SOC_{min}	30%
Inductance of each $Conv1_i$	L_1	500μH	Reference voltage for DC bus	V_{ref}	48V
Switching frequency for *Conv1i* and *Conv2i*	f_{sw}	10kHz	Initial Voltage of DC bus	V_{B0}	24V
Rated power of each PV panel	P^{PV}	500W_p	Lower limit on DC bus voltage	V_L	45.6V
Rated household load	P^{load}	200W	Higher limit on DC bus voltage	V_H	50.4
Battery capacity for each nanogrid	C	2400Wh	Droop Coefficient for $Conv1_i$	R_d	0.218Ω
Rated Charging current for the battery	I_{rated}	10A	Proportional and integral parameters ($Conv1_i$)	k_p,k_i	0.33, 15
Rated voltage of each battery	V^b	24V	Proportional and integral parameters ($Conv2_i$)	k_p ,k_i	0.5, 50

below specified tolerance and subsequent instability. In this situation, it is desirable that all household loads are shed and there is no power sharing with the common dc bus, until the batteries are recharged again when PV resources are available. In this situation, Conv1_i of all N nanogrids will be operating in mode 2 and Conv2_i of all N nanogrids will be operating in the MPPT mode.

V. RESULTS AND DISCUSSIONS

For the validation of the proposed scheme, various test cases are analyzed via simulations and hardware in the loop (HIL).

A. Simulation Results for Decentralized Control

Simulations are carried out on MATLAB/Simulink using physical models of the converters and control schematic shown in Fig. 2(a). Various parameters for simulation are shown in Table I. In order to have a better illustration of results, $P_i^{\text{PV}}(t)$ is assumed equal to $P_i^{\text{load}}(t)$ for test cases 1–3.

1) All Nanogrids Are Within Specified Thresholds of SOC: In order to validate the scenarios *a* and *b* of Section IV, batteries of all nanogrids are assumed to be within specified thresholds, i.e., $\text{SOC}_{\min} \leq \text{SOC}_i \leq \text{SOC}_{\max}\ \forall i = 1, 2, 3, 4$. This case is evaluated with and without communal load. Results for variations in bus voltage, current sharing among nanogrids, and accelerated simulations (0.5 h) for SOC_i are shown in Fig. 3(a) and (b). After starting transient, if there is no communal load, current sharing among the nanogrids is almost zero, i.e., each nanogrid is working independently, without supplying or demanding power from the dc bus. So, their SOCs remain constant in this region and distribution losses are zero, despite load requirements of each household is being fulfilled.

At $t = 0.025$ s, a communal load of 500 W is applied due to which voltage of the dc bus drops from 48 to 47.3 V and each nanogrid starts contributing for communal load based on its availability index, i.e., SOC_i value. Therefore, all nanogrids are supplying power based on the modified droop $K_d(R_d, \text{SOC}_i)$ given by (11) and Fig. 2(c) (mode 5). Consequently, the nanogrid with the highest SOC contributes more toward communal load and its SOC decreases at a rapid slope in comparison to other nanogrids ($\Delta\text{SOC}_1 = 1.92\%$ in comparison to $\Delta\text{SOC}_4 = 2.52\%$ at the end of the simulation). Moreover, as discussed by Jin *et al.* [24], *I–V* droop exhibits superior transient performance in comparison to other droop methods (e.g., *V–I* droop); therefore, the transition from one mode to other is smooth. From Fig. 3(a), it is evident that upon the application

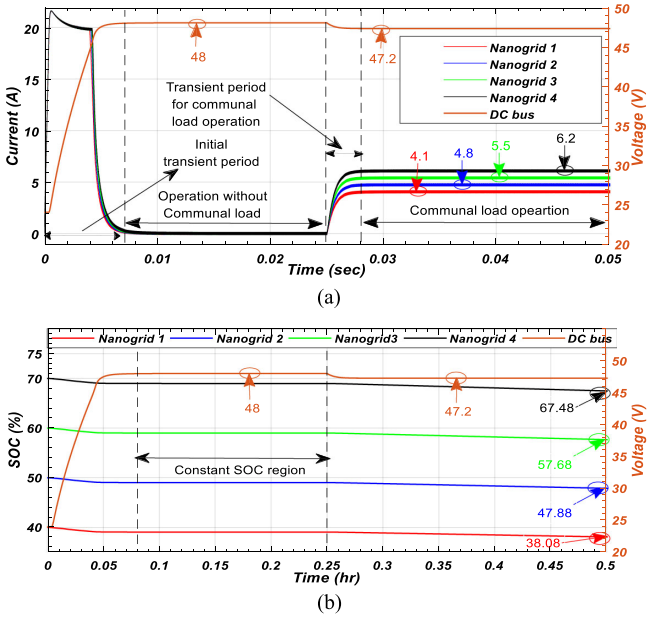

Fig. 3. (a) DC bus voltage V_B profile (right *Y*-axis) and current sharing among nanogrids (I_1^L, I_2^L, I_3^L, and I_4^L) (left *Y*-axis) in case 1 (simulation results). (b) DC bus voltage V_B profile (right *Y*-axis) and battery SOC for contributing nanogrids (SOC_1, SOC_2, SOC_3, and SOC_4) (left *Y*-axis) in case 1 (simulation results).

of communal load at $t = 0.025$ s, the proposed control achieves the new steady state in less than 0.005 s with negligible ringing or overshoot in converter current and dc bus voltage.

2) Two Nanogrids Are Within Specified Thresholds of SOC, While Remaining Two Are Below Threshold of SOC: In order to validate the scenarios *c* and *d* of Section IV, the batteries of two nanogrids are assumed to be within specified thresholds of SOC, while the batteries of remaining two nanogrids are assumed to be below threshold of SOC, i.e., $\text{SOC}_i < \text{SOC}_{\min}\ \forall i = 1, 2; \text{SOC}_{\min} \leq \text{SOC}_j \leq \text{SOC}_{\max}\ \forall j = 3, 4$. This case is evaluated with and without communal load, and results for variations in bus voltage, current sharing among contributing nanogrids, and accelerated simulations (0.5 h) for SOC_i are shown in Fig. 4(a) and (b), respectively.

Moreover, to visualize the accuracy of power sharing, two self-sufficient nanogrids are assumed to be having the same value of initial SOC, i.e., 70%. It can be seen that after starting transient, if there is no communal load, deficient nanogrids demand power in accordance to (4), also shown in Fig. 2(c)

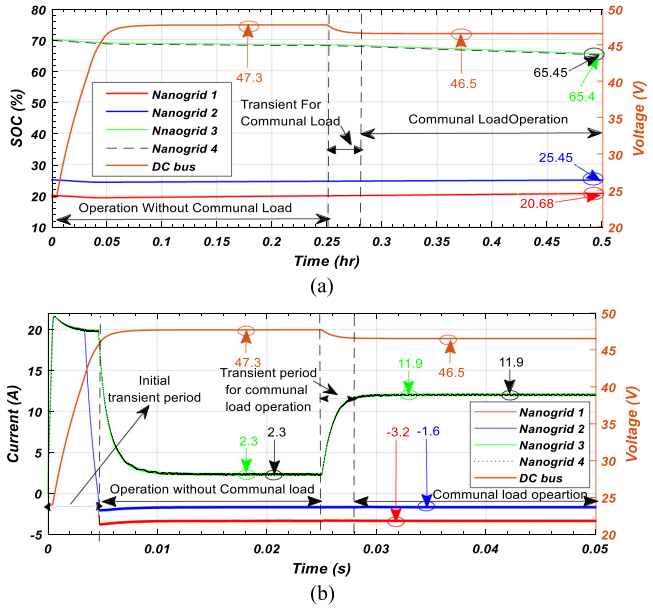

Fig. 4. (a) DC bus voltage V_B profile (right Y-axis) and current sharing among nanogrids (I_1^L, I_2^L, I_3^L, and I_4^L) (left Y-axis) in case 2 (simulation results). (b) DC bus voltage V_B profile (right Y-axis) and battery SOC for contributing nanogrids (SOC_1, SOC_2, SOC_3, and SOC_4) (left Y-axis) in case 2 (simulation results).

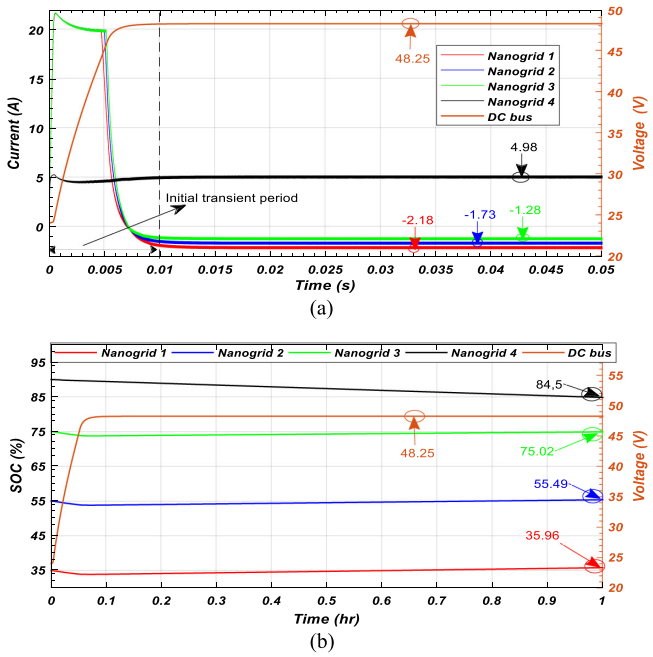

Fig. 5. (a) DC bus voltage V_B profile (right Y-axis) and current sharing among nanogrids (I_1^L, I_2^L, I_3^L, and I_4^L) (left Y-axis) in case 3 (simulation results). (b) DC bus voltage VB profile (right Y-axis) and battery SOC for contributing nanogrids (SOC_1, SOC_2, SOC_3, and SOC_4) (left Y-axis) in case 3 (simulation results).

(mode 1). Self-sufficient nanogrids supply power to the deficient nanogrids in accordance to (11) and Fig. 2(c) (mode 5).

Since power sharing is based on the SOC value only, therefore two nanogrids having the same value of SOC share exactly the same currents, as evident by overlapping lines in Fig. 4(a) and (b). At $t = 0.025$ s, a communal load of 500 W is applied due to which the voltage of the dc bus drops from 47.3 to 46.5 V and self-sufficient nanogrids start contributing for communal load as well as power demand of deficient nanogrids. Since deficient nanogrids demand power in proportion to their deficiency, thereby the nanogrid having a lower value of initial SOC is charged at higher current and vice versa ($\Delta\mathrm{SOC}_1 = 0.68\%$ in comparison to $\Delta\mathrm{SOC}_2 = 0.45\%$ at the end of the simulation).

3) All Nanogrids Are Within Specified Thresholds of SOC Except One, Which Is Above the Maximum Threshold of SOC: In order to validate the scenario *e* of Section IV, the batteries of three nanogrids are assumed to be within specified thresholds of SOC, while the battery of the fourth nanogrid is above the maximum threshold of SOC, i.e., $\mathrm{SOC}_{\min} \leq \mathrm{SOC}_j \leq \mathrm{SOC}_{\max}\ \forall i = 1, 2, 3; \mathrm{SOC}_4 > \mathrm{SOC}_{\max}$. Results for bus voltage profile, current sharing among contributing nanogrids, and accelerated simulations (1 h) for SOC_i are shown in Fig. 5(a) and (b).

Since the initial $\mathrm{SOC}_4^{(0)}$ is above threshold, i.e., 90%, therefore in this scenario, nanogrid 4 supplies power as dictated by (6), also shown in Fig. 2(c) (mode 3) with $I_1^L = 4.98$ A, while other three absorb power (their batteries are being charged) based on the modified droop $K_c(R_d, \mathrm{SOC}_i)$ given by (9) and Fig. 2(c) (mode 5).

It can be observed from Fig. 5(a) and (b) that power sharing via modified droop ensures resource distribution based on the availability index. Therefore, the nanogrid with initial $\mathrm{SOC}_3^{(0)} = 75\%$ (highest SOC and highest resource availability) is charged with the lowest current $I_3^L = -1.28$ A in comparison to the nanogrid with $\mathrm{SOC}_2^{(0)} = 55\%$ and the nanogrid with $\mathrm{SOC}_2^{(0)} = 35\%$, which are charged at $I_2^L = -1.73$ A and $I_3^L = -2.18$ A, respectively. Moreover, the changes in SOC_i from the start till the end of the simulation are also in accordance with the modified droop, such that the nanogrid with the highest resource availability is discharged at the highest rate, while nanogrid 3 with the minimum resources availability is charged at the lowest rate with $\Delta\mathrm{SOC}_1 = 0.96\%$, 0.49%, and 0.2% ($\Delta\mathrm{SOC}_1 < \Delta\mathrm{SOC}_2 < \Delta\mathrm{SOC}_3$).

4) Multimode Switching of an Individual Nanogrid: In order to realize the working of an individual nanogrid in all possible threshold ranges and to visualize the multimode switching based on the SOC thresholds, nanogrids 2–4 are considered to be working within specified maximum and minimum thresholds of SOC with $\mathrm{SOC}_2 < \mathrm{SOC}_3 < \mathrm{SOC}_4$, while nanogrid 1 is considered below threshold in the start of the simulation. It is assumed that PV power produced within the first three nanogrids is in accordance with their household loads, while incident irradiance and associated PV power produced within nanogrid 1 is higher than its household load requirements. Therefore, based on the energy balance given in (1) and (2), SOC_1 will increase from values below $\mathrm{SOC}_{\min}$ to values above $\mathrm{SOC}_{\max}$. Consequently, $\mathrm{Conv1}_1$ will switch its operating modes accordingly.

Fig. 6 shows the variations in current sharing among contributing nanogrids (I_1^L, I_2^L, I_3^L, and I_4^L) based on the accelerated SOC variations of an individual nanogrid (SOC_1). Accelerated SOC variations at nanogrid 1 are achieved by considering reduced battery capacity ($C/5$) and high incident irradiance (1000 W/m^2). It can be observed that when $\mathrm{SOC}_1 < \mathrm{SOC}_{\min}$, nanogrid 1 demands current with a negative value of

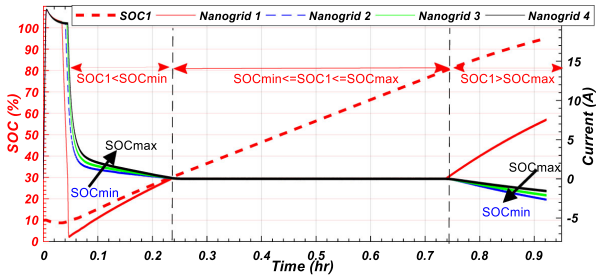

Fig. 6. Nanogrid 1 SOC_1 variation in the various thresholds ranges (left *Y*-axis) and associated current sharing among the contributing nanogrids in case 4 (right *Y*-axis) (simulation results).

I_1^L, as dictated by (4). Current demanded by nanogrid 1 I_1^L decreases as SOC increases and becomes almost zero, when it reaches to the minimum threshold point at $\mathrm{SOC}_1 = 30\%$ in accordance with Fig. 2(c) (mode 1). It is worth noting that within this range of operation, the current-supplying capability of the remaining three microgrids is governed by the modified discharging droop $K_d(R_d, \mathrm{SOC}_i)$ given by (11) and its visual representation is also shown in Fig. 2(c) (mode 5), such that nanogrid 4 having the highest SOC supplies the maximum current, while nanogrid 2 having the lowest SOC supplies lower current. In a mid-operation range, i.e., within specified limits of thresholds, all nanogrids share zero current; therefore, in this range, distribution losses are comparatively negligible. Also, it is evident from Fig. 6 that the intermode transition is very fast and smooth with the proposed strategy. For $\mathrm{SOC}_1 > \mathrm{SOC}_{\max}$, the nanogrid starts supplying current in accordance with (6) and mode 3 of Fig. 2(c); therefore, the value of I_L^1 keeps on increasing with the increase in SOC_1. In this mode of operation, the current sharing of remaining three microgrids is controlled by modified charging droop $K_c(R_d, \mathrm{SOC}_i)$ given by (9) and its visual representation is also shown in Fig. 2(c) (mode 5).

5) All Nanogrids are Above the Maximum Threshold of SOC and Surplus PV Power is Available: To validate the scenario f of Section IV, it is considered that all the nanogrids are above the maximum threshold and surplus PV power is available due to high incident irradiance (1000 W/m^2), i.e., $\mathrm{SOC}_i > \mathrm{SOC}_{\max}\ \forall i = 1, 2, 3, 4$. Each nanogrid will tend to supply power to the dc bus based on (6); therefore, its voltage will rise until it reaches to V_H. At V_H, the proposed droop function given by (7), also shown in Fig. 2(c) (mode 4), will reduce the current supply to zero and will try to keep the voltages fixed at V_H. Since the batteries are already above the maximum threshold, therefore any local PV generation P_i^{PV}, higher than local household requirements P_i^{load}, will overcharge the battery and cause dc bus voltage to rise above the maximum limit V_H, thus instigating instability in the system. At this point, the control schematic of $\mathrm{Conv2}_i$ changes its control from MPPT to inner loop current control mode, as shown in Fig. 2(c). Therefore, the *I–V* droop control mode (constant droop coefficient R_d) of $\mathrm{Conv1}_i$ stabilizes the dc bus voltage at V_H and $\mathrm{Conv2}_i$ ensures stability by culminating generation capability of each nanogrid according to the load requirements at individual household level. Fig. 7(a) shows that when dc bus voltage is below maximum threshold V_H, each nanogrid contributes for current according to its SOC_i. Once the voltage reaches to V_H, current contribution from each nanogrid becomes zero, and further rise

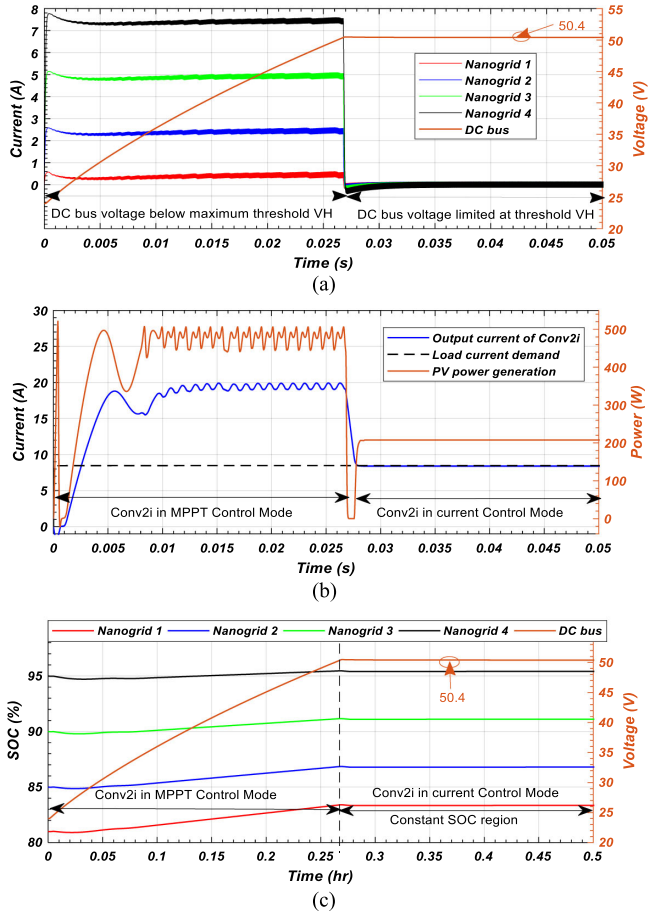

Fig. 7. (a) DC bus voltage V_B profile (right *Y*-axis) and current sharing among nanogrids (I_1^L, I_2^L, I_3^L, and I_4^L) (left *Y*-axis) in case 5 (simulation results). (b) Power generated by PV panels in nanogrid 1 P_1^{PV} (right *Y*-axis) and output current I_1^{in} of $\mathrm{Conv2}_1$ (left *Y*-axis) in case 5 (simulation results). (c) DC bus voltage V_B profile (right *Y*-axis) and battery SOC for contributing nanogrids (SOC_1, SOC_2, SOC_3, and SOC_4) (left *Y*-axis) in case 5 (simulation results).

in voltage is restricted to V_H. Before attaining V_H, each $\mathrm{Conv2}_i$ is operating in the MPPT mode, thus extracting the maximum power (500 W at incident irradiance of 1000 W/m^2). However, once dc bus voltage attains its maximum value V_H, the PV generation is limited according to household load requirements.

This is shown in Fig. 7(b), where $\mathrm{Conv2}_1$ of nanogrid 1 works in the MPPT (P&O) mode and generates power around 500 W in the start of the simulation. At $t = 0.027$ s, V_B reaches to its maximum allowable limit; therefore, $\mathrm{Conv2}_i$ shifts is control from MPPT to the current control mode, and therefore, the output current of $\mathrm{Conv2}_i$, i.e., I_1^{in} coincides with load current I_1^{PV} waveform, as shown in Fig. 7(b). This has been also shown in Fig. 7(c), where SOC_i of each converter increases due to PV generation higher than load requirements, when V_B is below V_H. After V_B becomes equal to V_H, due to change in the control mode of $\mathrm{Conv2}_1$ and associated limited PV generation, SOC of the battery does not rise any further and becomes constant onwards.

6) All Nanogrids Are Below Threshold of SOC and PV Generation is Not Available: In order to validate the scenario g of Section IV, In this case, the batteries of all nanogrids are assumed to be below the threshold level and PV generation is not

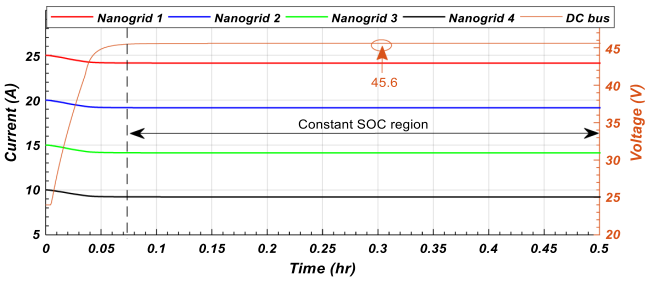

Fig. 8. DC bus voltage V_B profile (right *Y*-axis) and battery SOC for contributing nanogrids ($\mathrm{SOC}_1, \mathrm{SOC}_2, \mathrm{SOC}_3$, and SOC_4) (left *Y*-axis) in case 6 (simulation results).

available, i.e., $\mathrm{SOC}_i < \mathrm{SOC}_{\min}\ \forall i = 1, 2, 3, 4$. Since PV generation is not available and all the batteries are already below minimum threshold $\mathrm{SOC}_{\min}$, therefore any local load demand can further discharge batteries and cause dc bus voltage to collapse below minimum threshold level V_L. Therefore, all the local loads are turned OFF under this condition through a relay, and dc bus voltage is limited to lower threshold of voltage V_L through *I–V* droop with a constant droop coefficient given by (5) and also shown in Fig. 2(c) (mode 2). Thus, any further power sharing among the contributing nanogrids is restricted to maintain the bus voltage level and battery $\mathrm{SOC_i}$ level of individual batteries, as shown in Fig. 8. This condition is maintained until PV irradiance and associated PV generation are available again to charge the batteries above $\mathrm{SOC}_{\min}$.

B. Experimental Results for the Validation of the Proposed Adaptive Algorithm for Conv1$_{\mathrm{i}}$

In order to validate the proposed decentralized control scheme, HIL experimentation is conducted using Danfoss converters and dSpace RTI 1006 platform capable to perform real-time data acquisition and control operations [29]. The functioning of the adaptive algorithm for the control of $\mathrm{Conv1}_i$[shown in Fig. 2(c)] is evaluated, whose schematics and hardware setup are shown in Fig. 9(a) and (b), respectively. PV power is emulated using power supply, and the battery model is emulated using (1) and (2). Since functioning of $\mathrm{Conv2}_i$ is to ensure optimal PV generation while in the current setup PV power is being emulated, therefore control of $\mathrm{Conv2}_i$ is not implemented for experimentation. Various parameters of experimentations are further detailed in Table II.

1) All Nanogrids Are Within Specified Thresholds of SOC: In this scenario, the batteries of all nanogrids are assumed to be within specified thresholds of SOC, i.e., $\mathrm{SOC}_{\min} \leq \mathrm{SOC}_i \leq \mathrm{SOC}_{\max}\ \forall i = 1, 2, 3$. This case is evaluated with and without communal load of 135 W, and results for variations in bus voltage, current sharing among contributing nanogrids, and accelerated simulations (1 h) for SOC_i are shown in Fig. 10(a) and (b). Measured results are in accordance with the simulation results as without communal load; the current sharing among the contributing nanogrids is almost zero (slightly higher than zero due to equivalent series resistance (ESR) of individual capacitors, which otherwise was zero in case of simulation result due to an ideal capacitor). Upon application of communal load, the current sharing is in proportion to the SOC_i value. For instance, the battery of nanogrid 1 with initial $\mathrm{SOC}_1^0 = 35\%$ supplies 0.79 A, nanogrid 2 with initial $\mathrm{SOC}_2^0 = 55\%$ supplies 1.05 A, and nanogrid 3 with initial $\mathrm{SOC}_3^0 = 75\%$ supplies 1.33 A for communal load application.

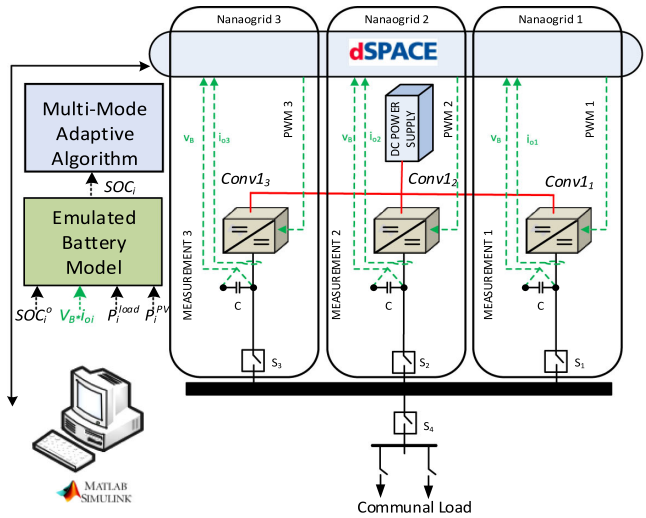

(a)

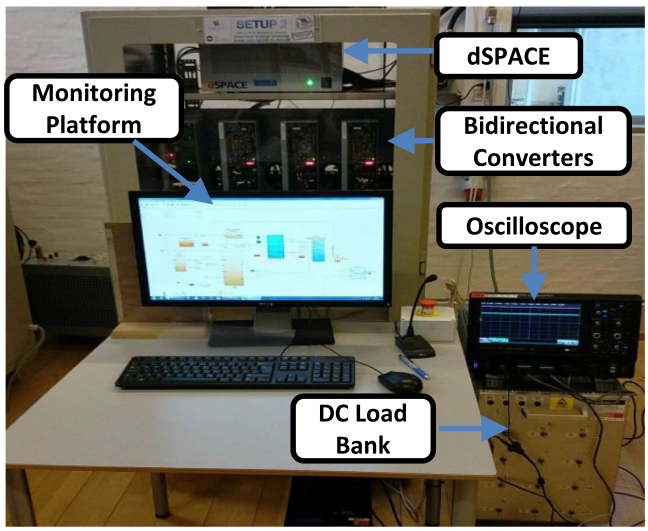

(b)

Fig. 9. (a) Schematics of the experimental setup at the Microgrid Laboratory. (b) Hardware setup for practical measurements.

The change in SOC is also in accordance with the SOC availability, i.e., $\Delta\mathrm{SOC}_1 = 0.49\%, \Delta\mathrm{SOC}_2 = 0.66\%$, and $\Delta\mathrm{SOC}_3 = 0.84\%$. Also, the initial transition and transition from no load to communal load scenario is fast and smooth, as shown in Fig. 10(a) and (b), respectively.

2) All Nanogrids Are Within Specified Thresholds of SOC Except One, Which Is Above the Maximum Threshold of SOC: In this scenario, the batteries of three nanogrids are assumed to be within specified thresholds of SOC, while the battery of the fourth nanogrid is the above maximum threshold, i.e., $\mathrm{SOC}_{\min} \leq \mathrm{SOC}_j \leq \mathrm{SOC}_{\max}\ \forall i = 2, 3; \mathrm{SOC}_1 > \mathrm{SOC}_{\max}$. Results for bus voltage profile, current sharing among contributing nanogrids, and accelerated simulations (1 h) for SOC_i are shown in Fig. 11(a) and (b). Results verify that nanogrid 1 having SOC higher than the maximum threshold is the supplying nanogrid,

TABLE II
PARAMETERS OF EXPERIMENTAL CASE STUDY

Description of the Parameter	Symbol	Value	Description of the Parameter	Symbol	Value
No. of Nanogrids/ households	N	3	Maximum threshold of battery *SOC*	SOC_{max}	80%
DC bus capacitance	C_B	3.3mF	Minimum threshold of battery *SOC*	SOC_{min}	30%
Inductance of each $Conv1_i$	L_1	8.6H	Reference voltage for DC bus	V_{ref}	48V
Stray resistance for Inductors	r_i	0.1Ω	Initial Voltage of DC bus	V_{B0}	24V
Switching frequency for $Conv1i$	f_{sw}	10kHz	Lower limit on DC bus voltage	V_L	45.6V
Rated power of each PV panel	P^{PV}	500W_p	Higher limit on DC bus voltage	V_H	50.4V
Rated household load	P^{load}	200W	Proportional and integral parameters ($Conv1_i$)	k_p,k_i	0.02, 0.1
Battery capacity for each nanogrid	C	2400Wh	Droop Coefficient for $Conv1_i$	R_d	0.25Ω
Rated charging current for battery	I_{rated}	5A			

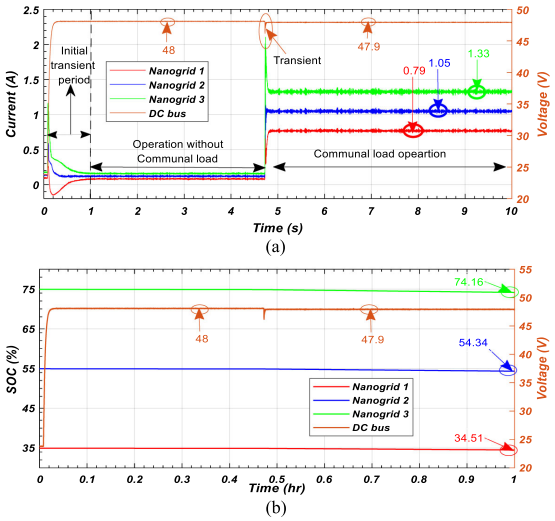

Fig. 10. (a) DC bus voltage V_B profile (right *Y*-axis) and current sharing among nanogrids (I_1^L, I_2^L, and I_3^L) (left *Y*-axis) in case 1 (measured results). (b) DC bus voltage V_B profile (right *Y*-axis) and battery SOC for contributing nanogrids (SOC_1, SOC_2, SOC_3, and SOC_4) (left *Y*-axis) in case 1 (measured results).

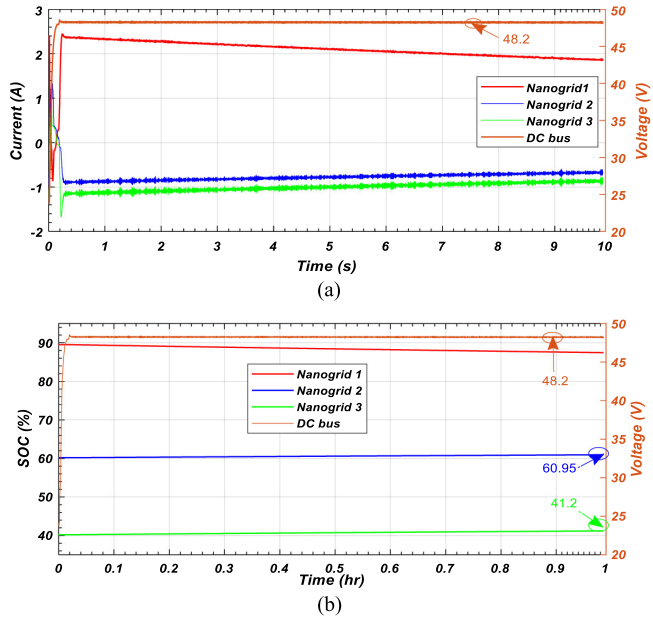

Fig. 11. (a) DC bus voltage V_B profile (right *Y*-axis) and current sharing among nanogrids (I_1^L, I_2^L, and I_3^L) (left *Y*-axis) in case 2 (measured results). (b) DC bus voltage V_B profile (right *Y*-axis) and battery SOC for contributing nanogrids (SOC_1, SOC_2, SOC_3, and SOC_4) (left *Y*-axis) in case 2 (measured results).

while remaining two nanogrids demand according to their resource availability.

Nanogrid 2 with the higher value of initial $SOC_2^0 = 60\%$ absorbs relatively lower current in comparison to nanogrid 3 having the higher value of initial $SOC_2^0 = 40\%$. Therefore, the change in SOC for absorbing nanogrids from the start till the end of the simulation is in accordance with resource availability, i.e., $\Delta SOC_2 = 0.95\%$ and $\Delta SOC_3 = 1.2\%$ with $(\Delta SOC_3 > \Delta SOC_2)$.

3) Multimode Switching of an Individual Nanogrid: Nanogrids 2 and 3 are considered to be working within specified maximum and minimum thresholds of SOC with $SOC_2 < SOC_3$, while nanogrid 1 is considered below threshold in the start of the simulation. It is assumed that PV power produced within nanogrids 2 and 3 is in accordance with their household load, while PV power produced within nanogrid 1 is higher than its household load requirements. Therefore, based on the emulated model of the battery, SOC_1 will increase from values below SOC_{min} to values above SOC_{max}, and $Conv1_1$ will switch its operating modes accordingly.

Fig. 12 shows the variations in current sharing among contributing nanogrids (I_1^L, I_2^L, and I_3^L) based on the accelerated SOC variations of an individual nanogrid (SOC_1). Accelerated

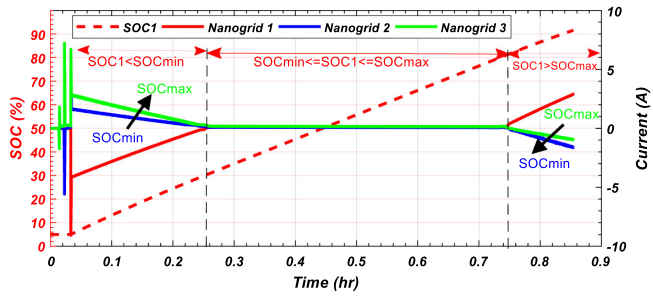

Fig. 12. Nanogrid 1 SOC_1 variations in the various threshold ranges (left *Y*-axis) and associated current sharing among the contributing nanogrids (right *Y*-axis) in case 3 (measured results).

SOC variations at nanogrid 1 are achieved by considering reduced battery capacity (C/10). From Fig. 12, it can be observed that for region $SOC_1 < SOC_{min}$, nanogrid 1 demands current with the negative value of I_1^L and nanogrids 2 and 3 supply in proportion to their SOC; therefore, the battery of nanogrid 3 having initial $SOC_3^{(0)} = 60\%$ supplies more current in this re-

gion in comparison to nanogrid 2 having $\mathrm{SOC}_2^{(0)} = 40\%$. This is in accordance with the simulation results shown in Fig. 6 and *I–V* droop function, as shown in Fig. 2(c) (mode 5). The slope of droop increases with SOC in this particular region, as shown by the arrow in Fig. 12, which is in accordance with equation discharging droop coefficient $K_d(\mathrm{SOC}_i, R_d)$ given by (11). For the intermediate region, the current contribution from each nanogrid becomes zero; therefore, it also validates our consideration of almost zero distribution losses in the range of $\mathrm{SOC}_{\min} \leq \mathrm{SOC}_i \leq \mathrm{SOC}_{\max}$. Finally, in the region when $\mathrm{SOC}_i > \mathrm{SOC}_{\max}$, nanogrid 1 starts supplying current with the positive value of I_1^L, while nanogrids 2 and 3 absorb power in proportion to their resource deficiency. Current sharing is controlled by charging droop coefficient $K_c(\mathrm{SOC}_i, R_d)$ given by (9) and shown in Fig. 2(c) (mode 5), such that nanogrid 3 having $\mathrm{SOC}_3^{(0)} = 60\%$ absorbs less current in this region in comparison to nanogrid 2 having $\mathrm{SOC}_2^{(0)} = 40\%$.

VI. Conclusion

An adaptive *I–V* droop method for the decentralized control of a PV/battery-based distributed architecture of an islanded dc microgrid is presented and its validity is demonstrated with simulations and HIL experimentation. The stability of the islanded microgrid under critical operation conditions is ensured via controlled synchronization between generation resources and load requirements. The proposed control method is highly suitable for the rural electrification of developing regions because it

1) enables coordinated distribution of generation and storage resources at a village scale;
2) reduces distribution losses associated with the delivery of energy between generation and load end;
3) decentralized controllability omits the need of central controller and associated costly communication infrastructure;
4) enables resource sharing among the community to extract the benefit of usage diversity at a village scale.

Results have also shown that adaptive *I–V* droop algorithm enables fast and smooth transitions among various modes of microgrid operation based on the resource availability in individual households of the village. Therefore, the implementation of the proposed control method on the PV/battery-based DGDSA of the islanded dc microgrid will enable high efficiency and better resource utilization in future rural electrification implementations.

References

[1] World Energy Outlook, "Electricity access database," 2016. [Online]. Available: http://www.worldenergyoutlook.org/resources/energydevelopment/energyaccessdatabase/.

[2] K. Ubilla *et al.*, "Smart microgrids as a solution for rural electrification: Ensuring long-term sustainability through cadastre and business models," *IEEE Trans. Sustain. Energy*, vol. 5, no. 4, pp. 1310–1318, Oct. 2014.

[3] N. J. Williams, P. Jaramillo, J. Taneja, and T. S. Ustun, "Enabling private sector investment in microgrid-based rural electrification in developing countries: A review," *Renew. Sustain. Energy Rev.*, vol. 52, pp. 1268–1281, 2015.

[4] S. C. Bhattacharyya, "Financing energy access and off-grid electrification: A review of status, options and challenges," *Renew. Sustain. Energy Rev.*, vol. 20, pp. 462–472, 2013.

[5] J. J. Justo, F. Mwasilu, J. Lee, and J.-W. Jung, "AC-microgrids versus dc-microgrids with distributed energy resources: A review," *Renew. Sustain. Energy Rev.*, vol. 24, pp. 387–405, 2013.

[6] J. Khan and M. H. Arsalan, "Solar power technologies for sustainable electricity generation–A review," *Renew. Sustain. Energy Rev.*, vol. 55, pp. 414–425, 2016.

[7] K. Shenai, A. Jhunjhunwala, and P. Kaur, "Electrifying India: Using solar dc microgrids," *IEEE Power Electron. Mag.*, vol. 3, no. 4, pp. 42–48, Dec. 2016.

[8] P. A. Madduri, J. Poon, J. Rosa, M. Podolsky, E. A. Brewer, and S. R. Sanders, "Scalable dc microgrids for rural electrification in emerging regions," *IEEE J. Emerging Sel. Top. Power Electron.*, vol. 4, no. 4, pp. 1195–1205, Dec. 2016.

[9] S. Mishra and O. Ray, "Advances in nanogrid technology and its integration into rural electrification in India," in *Proc. Int. Power Electron. Conf.*, 2014, pp. 2707–2713.

[10] D. Palit, G. K. Sarangi, and P. Krithika, "Energising rural India using distributed generation: The case of solar mini-grids in Chhattisgarh state, India," in *Mini-Grids for Rural Electrification of Developing Countries*. New York, NY, USA: Springer, 2014, pp. 313–342.

[11] D. Palit and G. K. Sarangi, "Renewable energy based mini-grids for enhancing electricity access: Experiences and lessons from India," in *Proc. Int. Conf. Utility Exhib. Green Energy Sustain. Develop.*, Mar. 2014, pp. 1–8.

[12] J. Urpelainen, "Energy poverty and perceptions of solar power in marginalized communities: Survey evidence from Uttar Pradesh, India," *Renew. Energy*, vol. 85, pp. 534–539, 2016.

[13] M. Nasir, N. A. Zaffar, and H. A. Khan, "Analysis on central and distributed architectures of solar powered dc microgrids," in *Proc. 2016 Clemson Univ. Power Syst. Conf.*, 2016, pp. 1–6.

[14] S. Groh, D. Philipp, B. E. Lasch, and H. Kirchhoff, "Swarm electrification-Suggesting a paradigm change through building microgrids bottom-up," in *Proc. 3rd Int. Conf. Develop. Renew. Energy Technol.*, 2014, pp. 1–2.

[15] W. Inam, D. Strawser, K. K. Afridi, R. J. Ram, and D. J. Perreault, "Architecture and system analysis of microgrids with peer-to-peer electricity sharing to create a marketplace which enables energy access," in *Proc. 9th Int. Conf. Power Electron. ECCE Asia*, 2015, pp. 464–469.

[16] P. A. Madduri, J. Rosa, S. R. Sanders, E. A. Brewer, and M. Podolsky, "Design and verification of smart and scalable dc microgrids for emerging regions," in *Proc. IEEE Energy Convers. Congr. Expo.*, 2013, pp. 73–79.

[17] P. A. Madduri, J. Poon, J. Rosa, M. Podolsky, E. Brewer, and S. R. Sanders, "Scalable dc microgrids for rural electrification in emerging regions," *IEEE J. Emerging Sel. Top. Power Electron.*, vol. 4, no. 4, pp. 1195–1205, Dec. 2016.

[18] J. Chi, W. Peng, X. Jianfang, T. Yi, and C. F. Hoong, "Implementation of hierarchical control in dc microgrids," *IEEE Trans. Ind. Electron.*, vol. 61, no. 8, pp. 4032–4042, Aug. 2014.

[19] T. Dragičević, J. M. Guerrero, J. C. Vasquez, and D. Škrlec, "Supervisory control of an adaptive-droop regulated dc microgrid with battery management capability," *IEEE Trans. Power Electron.*, vol. 29, no. 2, pp. 695–706, Feb. 2014.

[20] Q. Shafiee, T. Dragičević, J. C. Vasquez, and J. M. Guerrero, "Hierarchical control for multiple dc-microgrids clusters," *IEEE Trans. Energy Convers.*, vol. 29, no. 4, pp. 922–933, Dec. 2014.

[21] J. M. Guerrero, J. C. Vasquez, J. Matas, L. G. De Vicuña, and M. Castilla, "Hierarchical control of droop-controlled ac and dc microgrids—A general approach toward standardization," *IEEE Trans. Ind. Electron.*, vol. 58, no. 1, pp. 158–172, Jan. 2011.

[22] M. Nasir, H. A. Khan, A. Hussain, L. Mateen, and N. A. Zaffar, "Solar PV-based scalable dc microgrid for rural electrification in developing regions," *IEEE Trans. Sustain. Energy*, vol. 9, no. 1, pp. 390–399, Jan. 2018.

[23] X. Lu, K. Sun, J. M. Guerrero, J. C. Vasquez, and L. Huang, "State-of-charge balance using adaptive droop control for distributed energy storage systems in dc microgrid applications," *IEEE Trans. Ind. Electron.*, vol. 61, no. 6, pp. 2804–2815, Jun. 2014.

[24] Z. Jin, L. Meng, and J. M. Guerrero, "Comparative admittance-based analysis for different droop control approaches in dc microgrids," in *Proc. IEEE 2nd Int. Conf. DC Microgrids*, 2017, pp. 515–522.

[25] F. Gao *et al.*, "Comparative stability analysis of droop control approaches in voltage-source-converter-based dc microgrids," *IEEE Trans. Power Electron.*, vol. 32, no. 3, pp. 2395–2415, Mar. 2017.

[26] B. Subudhi and R. Pradhan, "A comparative study on maximum power point tracking techniques for photovoltaic power systems," *IEEE Trans. Sustain. Energy*, vol. 4, no. 1, pp. 89–98, Jan. 2013.
[27] M. Nasir and M. F. Zia, "Global maximum power point tracking algorithm for photovoltaic systems under partial shading conditions," in *Proc. 16th Int. Power Electron. Motion Control Conf. Expo.*, 2014, pp. 667–672.
[28] M. Nasir, S. Iqbal, and H. A. Khan, "Optimal planning and design of low-voltage low-power solar dc microgrids," *IEEE Trans. Power Syst.*, vol. 33, no. 3, pp. 2919–2998, May 2018.
[29] L. Meng, M. Savaghebi, F. Andrade, J. C. Vasquez, J. M. Guerrero, and M. Graells, "Microgrid central controller development and hierarchical control implementation in the intelligent microgrid lab of Aalborg University," in *Proc. IEEE Appl. Power Electron. Conf. Expo.*, 2015, pp. 2585–2592.

Mashood Nasir received the B.S. degree from the University of Engineering and Technology, Lahore, Pakistan, and the M.S. degree from the University of Management and Technology (UMT), Lahore, Pakistan, in 2009 and 2011, respectively, both in electrical engineering. Currently, he is working toward the Ph.D. degree at the Department of Electrical Engineering, Lahore University of Management Sciences, Lahore, Pakistan.

From 2011 to 2012, he was a Lecturer, and from 2013 to 2014, he was an Assistant Professor with the Electrical Engineering Department, UMT. From May 2017 to November 2017, he was a Visiting Ph.D. Researcher at the Microgrid Laboratory, Aalborg University, Aalborg, Denmark. His research interests mainly include but not limited to power electronics, electrical machines and drives, grid integration of alternate energy resources, electrochemical energy conversion, and battery storage systems and ac/dc/hybrid microgrids.

Zheming Jin (S'15) received the B.S. degree in electrical engineering and the M.S. degree in power electronics and ac drives from Beijing Jiaotong University, Beijing, China, in 2013 and 2015, respectively. He is currently working toward the Ph.D. degree in power electronic systems at the Department of Energy Technology, Aalborg University, Aalborg, Denmark.

His research interests include control of power electronic converters, stability of power electronic systems, energy storage, dc microgrids, and their applications in transportation electrification.

Hassan A. Khan (S'07–M'11) received the B.Eng. degree in electronic engineering from The Ghulam Ishaq Khan Institute of Engineering Sciences and Technology, Topi, Pakistan, in 2005, and the M.Sc. (with distinction) and Ph.D. degrees in electrical and electronic engineering from the School of Electrical Engineering, The University of Manchester, Manchester, U.K., in 2006 and 2010, respectively.

He is currently an Assistant Professor with the Department of Electrical Engineering, Lahore University of Management Sciences, Lahore, Pakistan. His current research is on renewable energy and its uptake in developing countries. His core focus is on novel grid architectures for low-cost rural electrification through solar energy. He is also working on efficient and reliable solar PV deployments in urban settings to maximize their performance ratios.

Nauman Ahmad Zaffar (M'10) received the B.S. and the M.S. degrees from University of Pennsylvania, in 1990 and 1991, respectively, both in electrical engineering. He is currently an Associate Professor and the Director of the Energy and Power Systems Research Cluster, Department of Electrical Engineering, Syed Babar Ali School of Science and Engineering, Lahore University of Management Sciences, Lahore, Pakistan. His research interests include smart grids and power electronic converters for integration of renewable energy resources and motor loads with an increasingly smarter grid. His primary research focus is on harnessing and efficient utilization of energy from available sources such as solar PV, solar thermal, wind, and hydrokinetics to enable energy independent, integrated, smart grid communities. He has been actively engaged in arranging and delivering national workshops in core areas of circuits, electronics, power electronics, and design of magnetics.

Juan C. Vasquez (M'12–SM'14) received the B.S. degree in electronics engineering from the Autonomous University of Manizales, Manizales, Colombia, and the Ph.D. degree in automatic control, robotics, and computer vision from the Technical University of Catalonia, Barcelona, Spain, in 2004 and 2009, respectively.

He was with the Autonomous University of Manizales, as a Teaching Assistant, and the Technical University of Catalonia, as a Post-Doctoral Assistant, in 2005 and 2008, respectively. In 2011, he was an Assistant Professor, and from 2014, he was an Associate Professor with the Department of Energy Technology, Aalborg University, Aalborg, Denmark, where he is the Vice Program Leader of the Microgrids Research Program (see microgrids.et.aau.dk). From February 2015 to April 2015, he was a Visiting Scholar with the Center of Power Electronics Systems, Virginia Tech, and a Visiting Professor with Ritsumeikan University, Kyoto, Japan. He has authored and coauthored more than 100 technical papers only in microgrids in international IEEE conferences and journals. His current research interests include operation, advanced hierarchical and cooperative control, optimization and energy management applied to distributed generation in ac–dc microgrids, maritime microgrids, advanced metering infrastructures, and the integration of Internet of Things and cyber-physical systems into the smart grid.

Josep M. Guerrero (S'01–M'04–SM'08–F'15) received the B.S. degree in telecommunications engineering, the M.S. degree in electronics engineering, and the Ph.D. degree in power electronics from the Technical University of Catalonia, Barcelona, Spain, in 1997, 2000, and 2003, respectively.

Since 2011, he has been a Full Professor with the Department of Energy Technology, Aalborg University, Aalborg, Denmark, where he is responsible for the Microgrid Research Program. Since 2012, he has been a Guest Professor with the Chinese Academy of Science, Beijing, China, and the Nanjing University of Aeronautics and Astronautics, Nanjing, China; since 2014, he has been the Chair Professor with Shandong University, Jinan, China; since 2015, he has been a Distinguished Guest Professor with Hunan University, Changsha, China; and since 2016, he has been a Visiting Professor Fellow with Aston University, Birmingham, U.K. His research interests are oriented to different microgrid aspects, including power electronics, distributed energy-storage systems, hierarchical and cooperative control, energy management systems, smart metering, and the Internet of things for ac–dc microgrid clusters and islanded minigrids; current research interests are especially focused on maritime microgrids for electrical ships, vessels, ferries, and seaports.

Dr. Guerrero is an Associate Editor for the IEEE TRANSACTIONS ON POWER ELECTRONICS, the IEEE TRANSACTIONS ON INDUSTRIAL ELECTRONICS, and the IEEE INDUSTRIAL ELECTRONICS MAGAZINE, and an Editor for the IEEE TRANSACTIONS ON SMART GRID and the IEEE TRANSACTIONS ON ENERGY CONVERSION. He was the Chair of the Renewable Energy Systems Technical Committee of the IEEE Industrial Electronics Society. He was a recipient of the IEEE TRANSACTIONS ON ENERGY CONVERSION Best Paper Award for the period 2014–2015, and the Highly Cited Researcher Award by Thomson Reuters in 2014 and 2015.